Journal of Alloys and Compounds 509 (2011) 8756–8760

Contents lists available at ScienceDirect

Journal of Alloys and Compounds

journal homepage: www.elsevier.com/locate/jallcom

Infrared emissivities and microwave absorption properties of perovskite $Sm_{0.5}Sr_{0.5}Co_{1-x}Fe_xO_3$ ($0 \le x \le 0.5$)

Le Chen, Chunhua Lu*, Yuanzheng Zhao, Yaru Ni, Jianbin Song, Zhongzi Xu

State Key Laboratory of Materials-Oriented Chemical Engineering, Nanjing University of Technology, No. 5 Xin Mofan Road, Gulou District, Nanjing 210009, China

ARTICLE INFO

Article history:
Received 6 April 2011
Received in revised form 7 June 2011
Accepted 14 June 2011
Available online 21 June 2011

Keywords:
Iron incorporation
Electrical conductivity
Infrared emissivity
Microwave absorbing properties

ABSTRACT

$Sm_{0.5}Sr_{0.5}Co_{1-x}Fe_xO_3$ ($0 \le x \le 0.5$, SSCF) with perovskite-type structure has been successfully prepared by conventional solid-state reaction as a microwave and infrared multi-functional material. The effects of Fe incorporation on the structure, electrical conductivity, infrared emissivity and microwave-absorbing properties were investigated in detail. XRD results have shown that the perovskite structure of SSCF has an orthorhombic symmetry for $0 \le x \le 0.4$ and a cubic symmetry for 0.5, respectively. The incorporation of Fe in SSCF could contribute to the decrease of electrical conductivity, while the infrared emissivities are increased. Moreover, microwave-absorbing properties in the frequency range of 2–18 GHz at room temperature are sensitive to Fe content. The complex permittivity, complex permeability and electromagnetic loss tangent have suddenly a step change at a certain frequency and the step-change frequency position moves slightly to lower frequencies with Fe increased. The optimal reflection loss calculated from the measured permittivity and permeability is 29.33 dB at 7.97 GHz with a thickness of 2.0 mm.
© 2011 Elsevier B.V. All rights reserved.

1. Introduction

Microwave absorption materials draw considerable attention in recent decades due to their widespread applications in electromagnetic compatibility (EMC), electromagnetic interference (EMI) and stealth technology of aircraft [1–3]. Generally, metallic magnetic particles, ferromagnetic-conducting polymer or ferroelectric-conducting polymer composite materials have been functionalized as good microwave absorbers [4–9]. With the rapid development of detection technologies, the materials capable of radar and infrared stealth are essentially required. The coating with high reflection and low absorption can lead to low emissivity and better camouflage capability in the infrared wave-band. However, this coating will emerge in the radar detection. To meet the performance requirement of infrared materials in battlefield scenarios, it is necessary to find a multi-functional material with compatible camouflage capability for radar and infrared wave-band [10,11].

Perovskite-type structure oxides (ABO_3) are widely used as cathode materials [12–15], gas sensors [16,17], new catalysts [18–20], for their high electrical conductivity, high dielectric constant, and high catalytic activity, which depend upon the different types and contents of metals occupying in the A and B sites [21–23]. Rare earth alkalide manganites show potentiality for thermochromic devices in the infrared range due to their charge ordering or metal-insulator transitions, tunable around room temperatures [24,25]. $LaMnO_3$ systems doped by Sr at site A and Fe or Co, Ni at site B exhibit good microwave absorbing properties due to their special electromagnetism characteristic, especially colossal magnetoresistance effect. The optimal absorption peak appeared at about 25 dB for $La_{1-x}Sr_xMnO_3$ ($x = 0.4$) sample with the thickness of 2.25 mm [26]. Doping contents of Sr and B (B = Fe, Co, Ni) have an influence on the step-change frequency position to a certain extent of $La_{1-x}Sr_xMn_{1-y}B_yO_3$ [27].

Strontium-doped samarium cobaltate ($Sm_{1-x}Sr_xCoO_3$, SSC) and A, B site doped SSC are being actively developed as one of the most promising cathode materials, even replace the conventional $La_{1-x}Sr_xMnO_3$ and $La_{1-x}Sr_xCoO_3$ materials [28–32]. Their researches focused mainly on achieving lower thermal expansion coefficient (TEC) values, at the same time, no decline in electrochemical properties [33–37]. Based on our preliminary study, it can be found that the bandwidth of the sintered undoped SSC is too small to use as microwave absorption materials despite with excellent infrared emissivity. Thereby, it would be instructive to suggest that the A, B site doped compositions possess better absorbing characteristics when compared with the undoped one [27]. To our knowledge, there are not prior investigations on this aspect, especially on relation between doping concentration, structure, infrared emissivity and microwave absorbing properties of $Sm_{1-x}Sr_xCoO_3$ perovskite-type oxides. These observations were the motivation for our study to provide additional knowledge of these SSC perovskites. The adjustment of microwave-absorbing properties, which is one of the main challenges of SSC, could be achieved by doping transition metal (Fe, Co, Ni) substitution.

* Corresponding author. Tel.: +86 25 83587252; fax: +86 25 83587220.
E-mail addresses: njlch@hotmail.com, chhlu@njut.edu.cn (C. Lu).

0925-8388/$ – see front matter © 2011 Elsevier B.V. All rights reserved.
doi:10.1016/j.jallcom.2011.06.055

So the purpose of this study was to prepare $Sm_{0.5}Sr_{0.5}Co_{1-x}Fe_xO_3$ $(0 \le x \le 0.5)$ materials and investigate the influence of Fe incorporation on the structure, electrical conductivities, infrared emissivities and microwave-absorbing properties of these perovskites.

2. Experimental procedure

2.1. Sample preparation

$Sm_{0.5}Sr_{0.5}Co_{1-x}Fe_xO_3$ (SSCF) samples were prepared by conventional solid-state reaction. Sm_2O_3, $SrCO_3$, Co_2O_3 and Fe_2O_3 were mixed in a weight ratio calculated from the stoichiometric composition of $Sm_{0.5}Sr_{0.5}Co_{1-x}Fe_xO_3$. All the raw materials are chemical grade. The Fe^{3+} doping concentration (x) in the SSCF compounds is 0, 0.10, 0.20, 0.30, 0.40, and 0.50, respectively. Ethanol was added as a milling medium together with the raw materials. With several repeated ball milling and calcinations at 900 °C for 6 h, the samples of SSCF compounds pressed into discs with polyvinyl alcohol. The samples were subjected to sintering temperature of 1200 °C for 24 h.

2.2. Characterization

The crystal structure was analyzed by ARL X'TRA power X-ray diffraction system with Cu Kα radiation source (λ = 0.15406 nm) operated at 45 kV and 35 mA, and the scanning rate (2θ) of 10 °C min^{-1} was applied to record the pattern in the 2θ ranged from 20° to 80°.

The electrical conductivity of the SSCF materials was measured using the standard four-probe DC method. Rods of SSCF were sintered at 1200 °C for 5 h in air. Rectangular bars with approximate dimensions of 50 mm × 8 mm × 4 mm were obtained from the sintered rods. Ag lead was attached to the rod with Ag paste and fired at 600 °C for 30 min to obtain a firm bonding and good electrical contact between the Ag leads and the sample. Measurements were performed from room temperature to 550 °C with a heating rate of 5 °C min^{-1}.

The infrared emissivity (ε) in the wavelengths (3–30 μm) was measured by the Model AE1 (D&S Company, USA). The detector portion of the device is heated to 82 °C so that the measured sample could not be heated. It has been testified that the infrared emissivity shows the linear relation with voltage. So the infrared emissivity will be obtained after the detector is layed down on the surface of samples for 90 s.

The complex permittivity and permeability of the samples were measured by Agilent E8363C microwave vector network analyzer in the frequency range of 2–18 GHz.

3. Results and discussion

3.1. XRD

XRD patterns of $Sm_{0.5}Sr_{0.5}Co_{1-x}Fe_xO_3$ $(0 \le x \le 0.5)$ are shown in Fig. 1. All the diffraction peaks of $Sm_{0.5}Sr_{0.5}Co_{1-x}Fe_xO_3$ correspond to the characteristic peaks of $Sm_{0.5}Sr_{0.5}CoO_3$ (JCPDS file card No. 53-112). However, the diffraction peaks of $Sm_{0.5}Sr_{0.5}Co_{1-x}Fe_xO_3$ shift to lower angle with the increasing of Fe incorporation, suggesting that Fe^{3+} ions might have doped into the B-site of $Sm_{0.5}Sr_{0.5}CoO_3$, since Fe^{3+} (R_{III} = 0.645 Å) is larger than Co^{3+} (R_{III} = 0.61 Å). It also can be observed that the initial volume increases at room temperature with increasing iron content, as may result from the relative values of ionic radii of iron and cobalt cations in octahedral coordination [33]. The lattice parameters for $Sm_{0.5}Sr_{0.5}Co_{1-x}Fe_xO_3$ $(0 \le x \le 0.5)$ are summarized in Table 1.

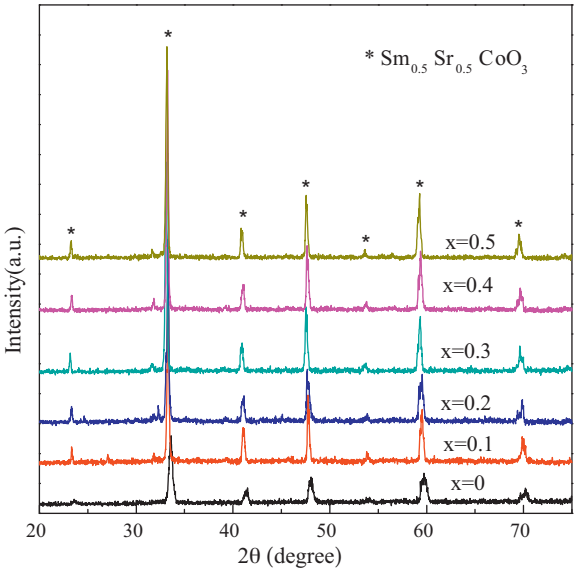

Fig. 1. XRD patterns of $Sm_{0.5}Sr_{0.5}Co_{1-x}Fe_xO_3$ $(0 \le x \le 0.5)$.

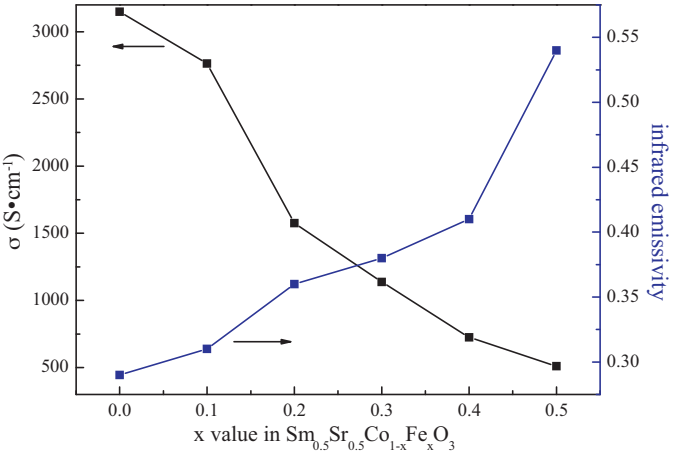

Fig. 2. Composition dependence of the electrical conductivity and infrared emissivity for $Sm_{0.5}Sr_{0.5}Co_{1-x}Fe_xO_3$.

3.2. Electrical conductivities and infrared emissivities

The electrical conductivities of SSCF ceramics are dominated by p-type electronic conduction. The conductivity of this system depends upon the incorporation of Fe, since the doping concentration determines the carrier (hole) concentration. The undoped SSC reaches a maximum value of 3149.64 S cm^{-1}. Thereafter, the electrical conductivity of SSCF gradually decreases with increasing of Fe (x = 0.1–0.5), as illustrated in Fig. 2. In the vicinity of Fe doping level x = 0.2 ($Sm_{0.5}Sr_{0.5}Co_{0.8}Fe_{0.2}O_3$), the conductivity shows a remarkable variation. The fast decrease in conductivity at higher doping level could be due to the formation of a significant amount of Fe^{4+} ions with poor capacity to conduct electricity. Preferential electronic charge compensation $Fe^{3+} \rightarrow Fe^{4+}$ over $Co^{3+} \rightarrow Co^{4+}$ most likely takes place in SSCF, resulting in a decrease in the electrical conductivity [32].

Table 1
The cell parameters of $Sm_{0.5}Sr_{0.5}Co_{1-x}Fe_xO_3$ $(0 \le x \le 0.5)$.

x	Crystal structure	a (Å)	b (Å)	c (Å)	Volume (Å^3)
0	Orthorhombic	5.3369	7.5703	5.3679	216.87
0.1	Orthorhombic	5.3995 ± 0.0010	7.5848 ± 0.0017	5.3616 ± 0.0017	219.58
0.2	Orthorhombic	5.4183 ± 0.0027	7.5874 ± 0.0049	5.3649 ± 0.0014	220.56
0.3	Orthorhombic	5.4863	5.4746	7.7317	232.23
0.4	Orthorhombic	5.4863	5.4759	7.7107	231.65
0.5	Cubic	3.8179 ± 0.0023			55.65

In the thermal infrared wavelengths (3–30 μm), $h\nu < 0.2$ eV, photon energy is not enough to make transition of electrons between valence band and conductive band. The ε (emissivity of the object) was determined by the carrier density N, carrier mobility μ and carrier collision frequency ω together, while carrier concentration and mobility are strongly related to conductivity. The different infrared emissivity properties are thus expected under different doping concentration [38–40].

The composition dependences of infrared emissivity and electrical properties for all samples measured at room temperature are also displayed in Fig. 2. At appropriate Fe doping concentration, such as $0.1 \le x \le 0.3$, slight variation of ε of SSCF compounds is observed. The infrared emissivity increases significantly from 0.41 to 0.54 when the Fe doping concentration is from 0.4 to 0.5. The hybridization of Co–O–Co is disturbed by the introduction of Fe, and the introduced hole carriers show little itinerant. Thus when Fe replaces Co in SSCF, the transfer of carriers is obstructed near the Fe site. And the possibility of electron hopping (via the overlap between Co 3d electrons and the O 2p electrons) is much weaker near the Fe site than that near Co site, which could attribute to the decreased mobility of free electrons.

Here, we only investigate the infrared emissivity of SSCF at room temperature. Adapted from Ref. [32] and described in Ref. [40], materials with a low temperature, semiconductor like behavior, and a high temperature metallic state, with an adjustable transition temperature, are good candidates for thermal control devices in spacecrafts.

As mentioned above, the electrical conductivity plots versus inverse temperature measured from room temperature to 550 °C were performed in Fig. 3. The electrical conductivities obey the Arrhenius relationship, indicating that the mechanism of electronic transport is the hopping of p-type small polaron. The temperature dependent electrical conductivity of the small polaron materials is given by the following equation:

$$\sigma = \left(\frac{A}{T}\right) \exp\left(-\frac{E_a}{KT}\right)$$

where A, T, K, E_a are defined as the pre-exponential factor, the absolute temperature, the Boltzmann constant and the hopping activation energy, respectively. Electrical conductivities for each sample increase with increasing temperature in the whole temperature region, agreeing well with the previous observations [32,33]. According to above results, the emissivity of SSCF samples is expected to automatically self-adjust by changing the temperature. Temperature dependence infrared emissivities of SSCF are under study.

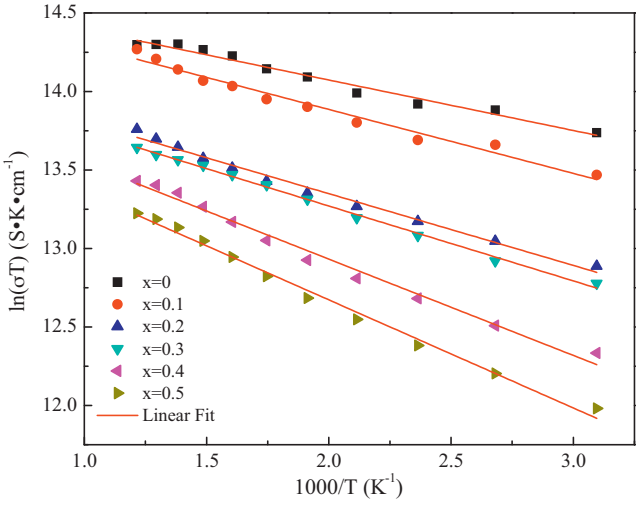

Fig. 3. Temperature dependence of the electrical conductivity for $Sm_{0.5}Sr_{0.5}Co_{1-x}Fe_xO_3$.

3.3. Microwave-absorbing properties

3.3.1. Permittivity and permeability spectra

The complex permeability ($\mu = \mu' - j\mu''$) and permittivity ($\varepsilon = \varepsilon' - j\varepsilon''$) of $Sm_{0.5}Sr_{0.5}Co_{1-x}Fe_xO_3$ ($0.1 \le x \le 0.5$) is sensitive to Fe content as shown in Figs. 4 and 5. The increase of dielectric loss (ε'') and dielectric constant (ε') is evident in Fig. 4. The peaks associated with the orthorhombic to cubic phase transition broaden gradually with increasing value of x. For SSCF, the real and imaginary parts of complex permeability are negligibly small as compared with that of complex permittivity, indicating that the dielectric loss mainly contributes to the reflection loss. The electrical conductivity changes considerably with Fe content, which results in distinct changes in dielectric constant. High value of dielectric constant is attributed to semi-conducting behavior of $Sm_{0.5}Sr_{0.5}Co_{1-x}Fe_xO_3$. The dielectric properties of SSCF arise mainly due to the interfacial polarization and intrinsic electric dipole polarization. The mechanism of intrinsic electric dipole polarization is considered as due to hopping electrons between Co^{3+} and Co^{4+}. While Fe^{3+} ions replace Co^{3+} ions, more iron hopping electrons will arise. Magnetic loss μ'' also increases with the Fe content and dispersion peak of μ'' moves slightly to lower frequency (from 12 GHz for $x = 0.1$ to 8 GHz for $x = 0.5$) as shown in Fig. 5(b). Notably, spectrum line corresponding to the strongest peak becomes comparatively sharp line with increase x values. The maximum permeability value exists at $x = 0.5$. The increase of μ'' suggests that the introduction of Fe enhance the magnetic loss of SSCF. An obvious second absorption peak can be found at 16.02 GHz, 17.28 GHz, 16.92 GHz for $x = 0.3$, 0.4, 0.5, respectively.

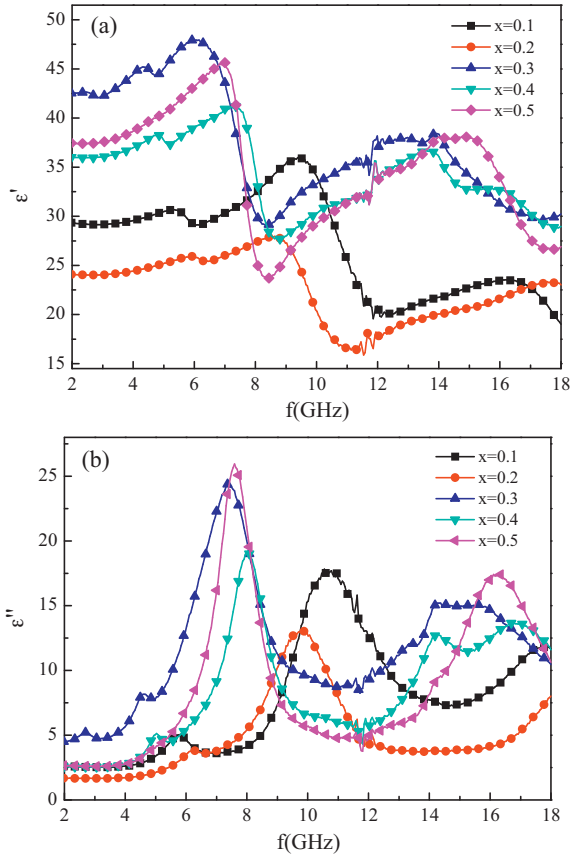

Fig. 4. Permittivity spectra of $Sm_{0.5}Sr_{0.5}Co_{1-x}Fe_xO_3$: (a) ε'; (b) ε''.

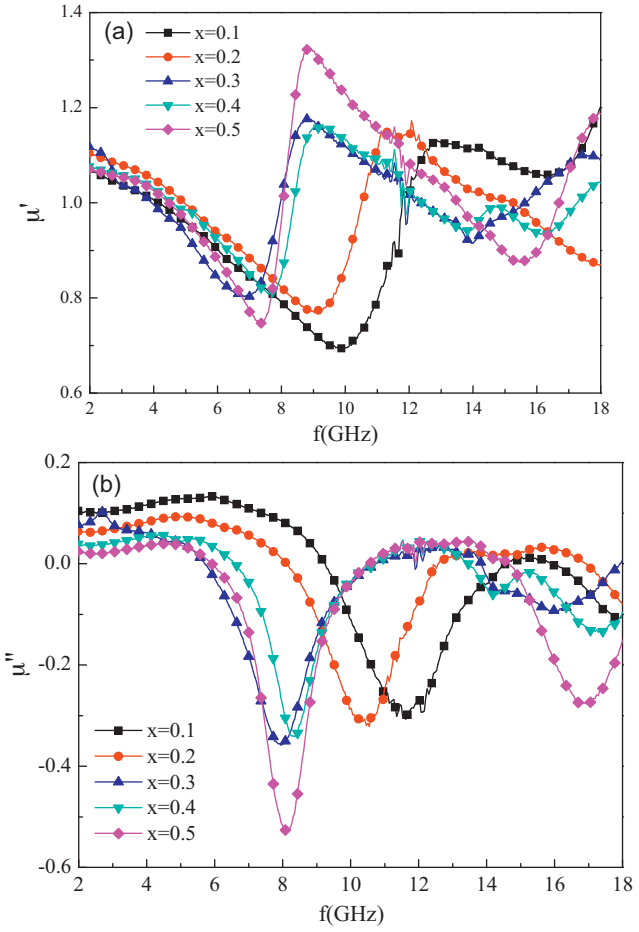

Fig. 5. Permeability spectra of $Sm_{0.5}Sr_{0.5}Co_{1-x}Fe_xO_3$: (a) μ'; (b) μ''.

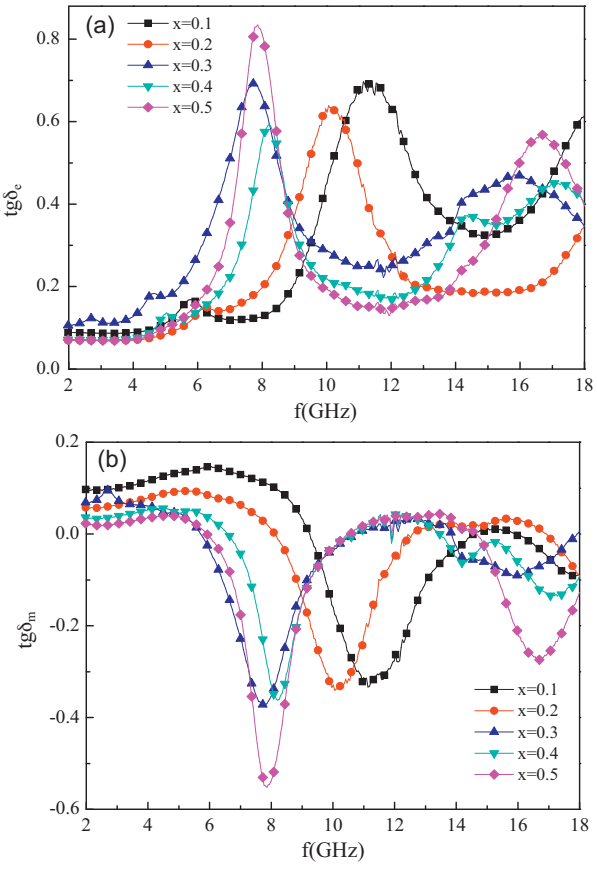

Fig. 6. Relationship between loss tangent and microwave frequency of $Sm_{0.5}Sr_{0.5}Co_{1-x}Fe_xO_3$: (a) $tg\delta_e$; (b) $tg\delta_m$.

3.3.2. Reflection loss

Different Fe doped $Sm_{0.5}Sr_{0.5}Co_{1-x}Fe_xO_3$ have the similar change for the dielectric and the magnetic spectra which suggests that their electromagnetism loss mechanism should be the same. Now, the electromagnetism loss mechanism of the materials will be explained by the characteristic change of loss tangent (loss factor) for SSCF.

A novel phenomenon is discovered that the electromagnetic loss tangent has suddenly a step change at a certain frequency, as presented in Fig. 6. The position of the step-change frequency varies for the different contents of Fe (12 GHz for $x = 0.1$ and 8 GHz for $x = 0.5$). When Fe concentration is 0.5, there is a sharp increase of loss tangent. The energy state of anti-ferromagnetic clusters could be linked with the content, which affects the potential barrier height between ferromagnetic clusters and anti-ferromagnetic clusters [27]. Besides, the microwave loss may also come from the resistive part [26]. The lower resistivity may arouse larger dielectric losses. This is consistent with Fig. 2 because $tg\delta_e$ for $x = 0.4$ sample is smaller than that of $x = 0.1$ sample.

At the thickness of 2.0 mm, the frequency dependence of the calculated reflection loss of SSCF in the frequency ranges of 2–18 GHz is shown in Fig. 7. It can be concluded that the high electrical conductivity gives rise to a high value of absorption. At 2–18 GHz, the specimen of $x = 0$ shows two broad bands at 8.91 and 12.73 GHz with −11.5 and −5.96 dB, while composite powders of $0.1 \le x \le 0.5$ show one broad band at the lower C-band frequencies. The $x = 0.1$ composite exhibits the largest reflection loss of −29.33 dB at 7.97 GHz and the widest bandwidth than those obtained from other specimens. Under the same matching thickness, the absorbing peak of $0.3 \le x \le 0.5$ becomes sharper and the maximum absorbing peak increases to −24.98 dB and shifts to 6.0 GHz for the change of impedance. For SSCF at low doping level, due to the Fe ions introduced into the parent compound SSC, Co^{3+} and Co^{4+} ions appear in the system. According to the double exchange model, the electron transfers between the Co^{3+} and Co^{4+} ions leading to the metallic conduction (hence lower resistivity) and ferromagnetism. The minimum reflection point shifts toward lower frequency after increasing the Fe content which might be due to higher magnetic loss as shown in (Fig. 5b). The difference in microwave absorbing properties of SSCF composites is due to the electric and magnetic losses generated by the magnetoelectric effects and by the changes of doping condition of the microwave field.

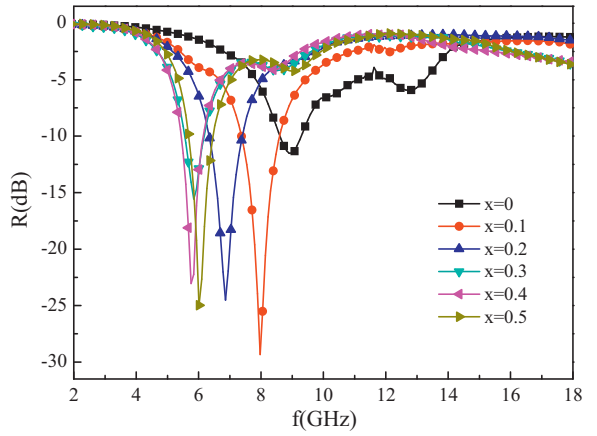

Fig. 7. Relationship between reflectance and microwave frequency of $Sm_{0.5}Sr_{0.5}Co_{1-x}Fe_xO_3$.

Generally, it is believed that the doping of Fe at B-site affects Co^{3+}–O–Co^{4+} to a certain extent and causes a break point on the electronic channel to reduce the quantity of electron jumping positions, which makes the resistivity increase to be in range of semiconductor. Such suitable conductivity and magnetic transformation will be beneficial to the materials absorbing microwave. Further studies on the relationship among the absorbing properties, electrical conductivity and magnetic domain structures of the compounds are in process.

4. Conclusions

$Sm_{0.5}Sr_{0.5}CoO_3$ has been selected for B site substitution with Fe to promote the microwave-absorbing properties. In this work, crystal structure, electrical conductivity, infrared emissivity and microwave absorption in the system $Sm_{0.5}Sr_{0.5}Co_{1-x}Fe_xO_3$ with $0 \le x \le 0.5$ were studied as function of Co/Fe ratio. SSCF for $0 \le x \le 0.4$ and $x = 0.5$ are identified as the orthorhombic symmetry phase and the cubic symmetry phase, respectively. More interesting, infrared emissivity is in agreement with the rapid decrease in electrical properties. The ε is tailored from 0.29 to 0.54 as the content of Fe is increased from 0 to 0.5. The microwave absorption measurements have confirmed that the higher the Fe content in $Sm_{0.5}Sr_{0.5}Co_{1-x}Fe_xO_3$, the higher the magnetic loss (μ'') and the lower the dispersion peak frequency. It is evident that the doped SSCF composites have much more effective electromagnetic absorption effects. The optimal absorption can be achieved and microwave loss peak is at 29.33 dB for $x = 0.1$ sample.

SSCF is provided with higher microwave absorption and a certain lower infrared emission, which suggest that it can be a promising candidate for a multi-functional material with compatible camouflage capability for radar and infrared wave-band.

Acknowledgement

This work was financially supported by the Innovation Scholars "Climbing" Program of Jiangsu Province (SBK200910148).

Appendix A. Supplementary data

Supplementary data associated with this article can be found, in the online version, at doi:10.1016/j.jallcom.2011.06.055.

References

[1] S.S. Kim, S.T. Kim, J.M. Ahn, et al., J. Magn. Magn. Mater. 271 (2004) 39–45.
[2] R.S. Meena, S. Bhattachrya, R. Chatterjee, J. Magn. Magn. Mater. 322 (2010) 1923–1928.
[3] Z. Xu, W. Lin, L.D. Kong, Prog. Electromagnet. Res. 69 (2007) 117–125.
[4] T. Maeda, S. Sugimoto, T. Kagotani, et al., J. Magn. Magn. Mater. 281 (2004) 195–205.
[5] Z.G. Fan, G.H. Luo, Z.G. Zhang, et al., Mater. Sci. Eng. B 132 (2006) 85–89.
[6] M.A. Soto-Oviedo, O.A. Araújo, R. Faez, et al., Synth. Met. 156 (2006) 1249–1255.
[7] T. Wang, J. He, J. Zhou, et al., J. Solid State Chem. 183 (2010) 2797–2804.
[8] C.C. Yang, Y.J. Gung, W.C. Hung, et al., Compos. Sci. Technol. 70 (2010) 466–471.
[9] C.C. Yang, Y.J. Gung, C.C. Shih, et al., J. Magn. Magn. Mater. 323 (2011) 933–938.
[10] B. Yu, L. Qi, J. Ye, et al., J. Appl. Polym. Sci. 104 (2007) 2180–2186.
[11] J. Zhou, J. He, G. Li, et al., J. Phys. Chem. C 114 (2010) 7611–7617.
[12] A.J. Jacobson, Chem. Mater. 22 (2010) 660–674.
[13] V.B. Vert, J.M. Serra, Fuel Cells 10 (2010) 693–702.
[14] U.F. Vogt, P. Holtappels, J. Sfeir, et al., Fuel Cells 9 (2009) 899–906.
[15] S.P. Jiang, J. Power Sources 124 (2003) 390–402.
[16] P. Song, Q. Wang, Z. Yang, Sens. Actuators B: Chem. 141 (2000) 109–115.
[17] Y. Itagaki, M. Mori, Y. Hosoya, et al., Sens. Actuators B: Chem. 122 (2007) 315–320.
[18] B.P. Barbero, J.A. Gamboa, L.E. Cadús, Appl. Catal. B 65 (2006) 21–30.
[19] J. Gao, X. Liu, D. Peng, et al., Catal. Today 82 (2003) 207–211.
[20] M.M. Natile, F. Poletto, A. Galenda, et al., Chem. Mater. 20 (2008) 2314–2327.
[21] Y. Zhang-Steenwinkel, H.L. Castricum, A. Bliek, et al., J. Mater. Sci. 42 (2007) 5851–5859.
[22] K. Vidal, L.M. Rodríguez-Martínez, L. Ortega-San-Martín, et al., Solid State Ionics 178 (2007) 1310–1316.
[23] J. Holc, D. Kuščer, M. Hrovat, et al., Solid State Ionics 95 (1997) 259–268.
[24] P. Laffez, C. Napierala, M. Zaghrioui, et al., Appl. Phys. Lett. 93 (15) (2008) 151910.
[25] P. Laffez, M. Zaghrioui, L. Reversat, et al., Appl. Phys. Lett. 89 (2006) 081909.
[26] G. Li, G. Hu, H. Zhou, et al., Mater. Chem. Phys. 75 (2002) 101–104.
[27] K. Zhou, D. Wang, K. Huang, et al., Trans. Nonferr. Metal. Soc. China 17 (2007) 1294–1299.
[28] S.S. Pawar, K.P. Shinde, R.S. Joshi, et al., Ionics 16 (2010) 649–654.
[29] H. Zhang, F. Zhao, F. Chen, et al., Solid State Ionics 192 (2011) 591–594.
[30] X. Lou, S. Wang, Z. Liu, et al., Solid State Ionics 180 (2009) 1285–1289.
[31] C. Zhu, G. Wang, J. Xue, et al., Acta Phys. Chim. Sin. 25 (2009) 2211–2217.
[32] H. Lv, B. Zhao, Y. Wu, et al., Mater. Res. Bull. 42 (2007) 1999–2012.
[33] H. Lv, Y. Wu, B. Huang, et al., Solid State Ionics 177 (2006) 901–906.
[34] S.W. Baek, J.H. Kim, J. Bae, Solid State Ionics 179 (2008) 1570–1574.
[35] Q. Xu, D. Huang, M. Chen, et al., J. Wuhan Univ. Technol.: Mater. Sci. Ed. 23 (2008) 386–390.
[36] F. Riza, Ch Ftikos, F. Tietz, et al., J. Eur. Ceram. Soc. 21 (2001) 1769–1773.
[37] H.Y. Tu, Y. Takeda, N. Imanishi, et al., Solid State Ionics 117 (1999) 277–281.
[38] F. Du, N. Wang, D. Zhang, et al., J. Rare Earth 28 (2010) 391–395.
[39] A.V. Moholkar, S.M. Pawar, K.Y. Rajpure, et al., J. Alloys Compd. 464 (2008) 387–392.
[40] K. Shimazaki, S. Tachikawa, A. Ohnishi, et al., Int. J. Thermophys. 22 (2001) 1549–1561.